



Linearization of wavelength sweeping lasers for the construction of 4-D FMCW LiDAR images of slow-moving objects using baseband beat note signals

YU-KUAN TSAI,^{1,2} ZHENG-XIANG LIAO,³ YU-XIANG LIN,⁴ H.-S. CHEN,⁵ JACK JIA-SHENG HUANG,⁵ PEI-HSUN WANG,^{3,6}  CHIA-CHIEN WEI,^{4,7}  YOU-CHIA CHANG,^{2,8}  YUNG HUNG JR.,⁴ AND JIN-WEI SHI^{1,9}

¹Department of Electrical Engineering, National Central University, Zhongli, 320, Taiwan

²Department of Photonics, National Yang Ming Chiao Tung University, Hsinchu, Taiwan

³Department of Optics and Photonics, National Central University, Taoyuan City 320317, Taiwan

⁴Department of Photonics, National Sun Yat-Sen University, Kaohsiung, Taiwan

⁵Source Photonics, No. 46, Park Avenue 2nd Rd., Science-Based Industrial Park, Hsinchu, Taiwan

⁶phwang@dop.ncu.edu.tw

⁷ccwei@mail.nsysu.edu.tw

⁸youchia@nycu.edu.tw

⁹jwshi@ee.ncu.edu.tw

Abstract: A FMCW LiDAR system of both the distributed feedback laser and external cavity laser is established in baseband beat notes, rather than up-conversion to an intermediate frequency to exclude flicker noise. Meanwhile, utilizing fast-scanning MEMS mirrors, high-quality real-time (1 fps) 4-D images of the slow-moving object (10 mm/s) can be directly constructed at the baseband with a central frequency as low as 100 kHz and a small Doppler shift. The proposed LiDAR architecture based on such a low-frequency baseband significantly improves the optical power budget on the transmitter side and eliminates the costly high-speed sampling circuits on the receiver side.

© 2024 Optica Publishing Group under the terms of the [Optica Open Access Publishing Agreement](#)

1. Introduction

Light Detection and Ranging (LiDAR) systems have experienced widespread adoption, transitioning beyond their traditional role in scientific applications such as meteorology [1] and space exploration [2]. Today, LiDAR has found versatile use in non-scientific domains, particularly in various industries, such as robotics applications [3] and autonomous vehicles [4,5]. Among the various LiDAR technologies, early researches focus on time-of-flight-based imaging by measuring the time period of a reflected light pulse [6], while more recent studies address frequency-modulated continuous wave (FMCW) LiDAR with potential 4-D imaging capability [7]. By mapping an object's distance and velocity into frequency with a frequency-chirped continuous wave (CW), optical self-heterodyne detection resolves the instantaneous velocity and distance from the reflected light of the target through the Doppler effect. 4-D (3D + velocity) imaging with ultra-high velocity sensitivity up to $\sim \mu\text{m}/\text{sec}$ has been recently demonstrated [8]. Such FMCW LiDAR has the potential for monitoring the vibration and deformation of mechanical structures [9]. To meet such a target, both the transmitter with high linearity in the wavelength sweeping process and the receiver with low phase noise of beat note signal are necessary. Several approaches have been proposed. Traditionally, a high-quality optical chirped waveform can be generated by utilizing a narrow linewidth laser and an external acoustic-optic modulator (AOM) [10] or an electro-optical modulator (EOM) [11], which is driven by a frequency sweeping

radio frequency (RF) source. These additional optical-to-electrical-to-optical (OEO) processes increase the cost and complicate the LiDAR system. Furthermore, the available optical power is usually limited by the insertion loss and maximum handling power of EOM instead of the laser itself. Another approach is to modulate the laser frequency directly. This can be accomplished by directly modulating a narrow linewidth light source, such as a distributed feedback (DFB) laser [12] or an external cavity diode laser (ECDL) [13]. By modulating carrier density inside the laser cavity, the frequency can be directly tuned, typically exhibiting a strong correlation with the output intensity [14], which is known as linewidth enhancement effect. Based on such method, a DFB laser under pulse current driving can serve as a high-performance wavelength sweeping light source in the 4-D FMCW LiDAR system with a high velocity sensitivity [15,16]. Besides, linearization processes are usually employed to compensate for the nonlinearity during such wavelength sweeping process through the pre-distortion of laser driving waveform [8,17]. The laser noise during wavelength sweeping process is also a critical issue for high-quality LiDAR images. In order to avoid the flicker noise ($1/f$) in laser light sources [18], typically from 0.1 Hz to a few kHz, various techniques can be employed, including signal processing algorithms, noise filtering methods, and improving the design and manufacturing processes of DFB lasers to minimize noise sources. An external modulator (MOD) has been proposed to be integrated with the sweeping light source for frequency up-conversion of beat note signal from the baseband to intermediate frequency (IF) [8,19]. Even exhibiting extremely high velocity sensitivity [8], the significant insertion loss (> 5 dB) and maximum handling optical power of MOD seriously degrade the optical power budget, which is an important issue for extending the ranging distance of LiDAR system. By installing an additional semiconductor optical amplifier (SOA) in the output of MOD thus becomes an attractive solution to compensate for its insertion loss [20,21]. However, this approach may degrade the signal-to-noise (S/N) ratio of the emitted light signal from LiDAR. A viable strategy to overcome these challenges is opting for a higher beat note frequency at the baseband, up to the MHz level, and eliminating the need for MOD [22]. Nevertheless, the cost of next-stage digital signal processing (DSP) ICs at high-frequency regimes tremendously increases. Therefore, there exists a strong desire to attain a high-quality (low phase/amplitude noise) baseband signal at the low-frequency regime (≈ 100 kHz) for direct 4-D image construction. Achieving this goal would eliminate the need for external modulation (MOD), enable the utilization of cost-effective DSP circuits, and bolster the optical power budget within the LiDAR system.

In this paper, we investigated the behaviors of both a DFB laser and an external cavity laser (ECL) under pre-distorted current modulation for the linearization of the wavelength-sweeping process. According to the measurement results, the optimized bias point for the wavelength-sweeping process happens at the most linear regime in the static L-I curves of both these two lasers. With such an operating condition, we can lower the frequency of the beat note signal at a baseband down to tens of kHz and effectively suppress its noise. A 4-D FMCW LiDAR system that works at low-frequency baseband has then been established further to evaluate the performance of both these two lasers for practical LiDAR applications. Compared with the DFB lasers as light sources, the ECL exhibits lower noise of the beat note signal on the receiver side, which leads to a much better quality of motion image at a low moving velocity (≈ 0.01 mm/s). By replacing the galvanometer (galvo) mirror with a fast-scanning microelectromechanical systems (MEMS) mirror in our LiDAR system, real-time (1 fps) 4-D LiDAR images of the slow-moving object (10 mm/s) can be obtained. Better image quality of velocity information can be realized by optimizing the MEMS scanning speed and refining the resolution along the fast axis. This scenery highlights the benefit of using baseband detection for high-resolution, real-time 4-D LiDAR images with high velocity sensitivity and opens a new way to have a simple, low-cost, and compact FMCW LiDAR system for novel applications.

2. System setup

Figure 1(a) shows the schematics of the FMCW LiDAR system. In this study, two different laser types – DFB laser chips (Source Photonics Taiwan, Inc.) and a commercial ECL (Thorlabs, SFL1550P) are used as the optical sources for our LiDAR system. A driving current pulse with a 1 kHz modulation frequency is utilized to directly modulate the laser for wavelength sweeping [8,15,22] based on the linewidth enhancement effect. The linearization process [8,17] of driving waveforms is applied to individual laser schemes, and the corresponding sensitivity of the LiDAR system will be studied. The output laser is directly sent into free space through a collimator. By scanning a pair of galvo mirrors (Thorlabs, GVSM002-US), the reflected light from objects is recorded by an optical p-i-n photodetector (Thorlabs, RXM42AF). The fiber length of the local arm is adjusted to ensure the beat notes at the low-frequency baseband with a central frequency at around tens to 100 kHz. We should note that, unlike the previous demonstration with the need of up-converting to an intermediated frequency, there is no need for a single-sideband (SSB) modulator [8,19] and the necessity of using costly high-speed signal processing ICs in the receiver end.

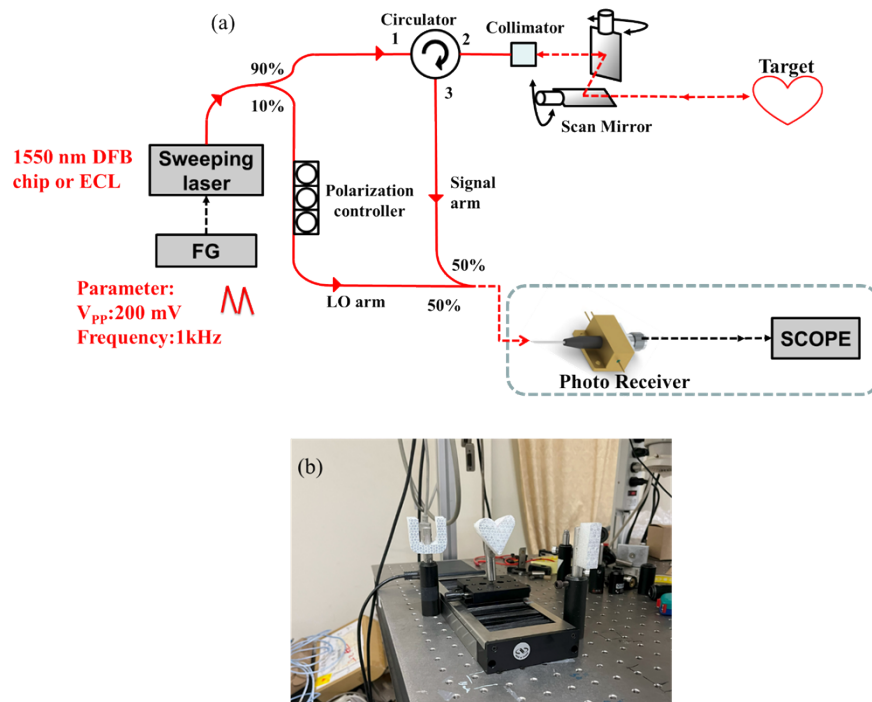


Fig. 1. (a) Schematic setup of FMCW LiDAR using baseband beat notes. (b) Setup of the I, \heartsuit , and U-shaped objects for the LiDAR measurement.

The examined targets comprised objects shaped as I, \heartsuit , and U, made from Styrofoam wrapped in retroreflective tape, as illustrated in Fig. 1(b). A motorized linear stage is utilized on the \heartsuit -shaped object at a given moving speed for velocity measurement, while the I and U-shaped objects remain static as that in Ref. [8]. The velocity image is acquired synchronously while the stage is moving forward to minimize uncertainties that may arise during the back-and-forth motion of the stage. A self-heterodyne scheme, as shown in Fig. 2, measures the sweeping frequency [23] to enable iterative linearization [17]. The iterative process entails discerning the difference between the actual sweeping frequency and the desired triangular frequency to

adjust the laser's driving waveform, aiming to optimize linearity. Initially utilizing a triangular waveform as the driving current, this iterative process progressively distorts it for a linear sweep. Within the self-heterodyne scheme, a modulated laser output is divided into two identical beams. A short time offset is introduced between them using a short fiber delay line, after which their beat note, detected by a balanced photodetector, unveils the frequency sweep. Specifically, the beat note's frequency corresponds to the frequency increment during the short time offset, allowing the accumulation of beating frequency to represent the sweeping frequency. Since frequency accumulation is synonymous with phase, the laser's frequency sweep can be directly deduced from the extracted beat note phase, obtained by applying the Hilbert transform to the detected beat note signal.

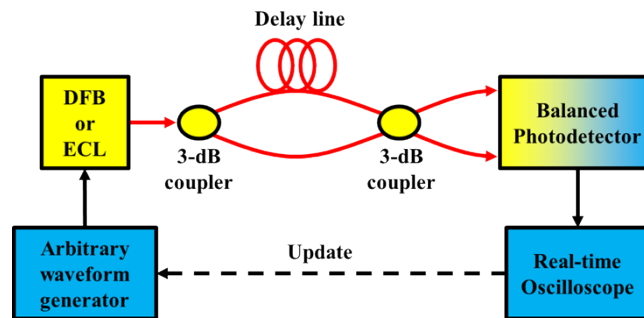


Fig. 2. Schematics of the self-heterodyne for linearity characterization during laser sweeping.

2.1. DFB laser characterization and 4-D LiDAR imaging

For the LiDAR demonstration with DFB laser chips, we first characterize the C-band DFB laser by coupling the light out of the facet with a lensed fiber as shown in Fig. 3(a). Figure 3(b) shows the corresponding light-current (L-I) curve of the exemplary DFB laser. Above the laser threshold, high linearity of L-I curve can be identified for < 200 mA driving currents, while power saturation appears for currents above 200 mA. The wavelength sweeping is then realized by triggering the driving current with a 1 kHz triangular waveform. From the slope efficiency (SE) of the L-I curve in Fig. 3(c), three different operating regimes of the driving current – close to the threshold ($I < 50$ mA), linear ($I = 50 \sim 150$ mA), and saturation ($I > 150$ mA), are studied for laser sweeping. A 5 m delayed fiber is used in the self-heterodyne scheme to keep the beat notes at the low-frequency baseband. Figures 4(a)-4(c) show the corresponding beat note frequency of self-heterodyne beating signals sweeping at 50 mA, 130 mA, and 280 mA driving currents, respectively. We can identify that beating signals with a constant frequency can only be realized at 130 mA, which is located at the plateau of the trace for SE vs. bias current. The corresponding differential quantum efficiency (DQE) is around 0.3 at 130 mA. In the meantime, the inadequate linearity observed during frequency sweeping at 50 mA and 280 mA laser bias currents results in distorted interference patterns on the oscilloscope, making it challenging to accurately determine the beating frequency via Fourier transform.

While it is possible to attain beating frequency at approximately 130 mA, the resulting beating signals at the baseband exhibit a slight chirp in frequencies. Ideally, the FMCW laser's instantaneous frequency should vary linearly to ensure a consistent beat note frequency. In order to achieve 4-D LiDAR images with high velocity sensitivity, we employ pre-distorted current modulation to linearize the wavelength-sweeping process [8,23], as discussed in Fig. 2. Figures 5(a)-5(d) show our iterative results during our linearization process of the beat note frequencies. The modulation current amplitude is set at around 50 mA, which ranges from

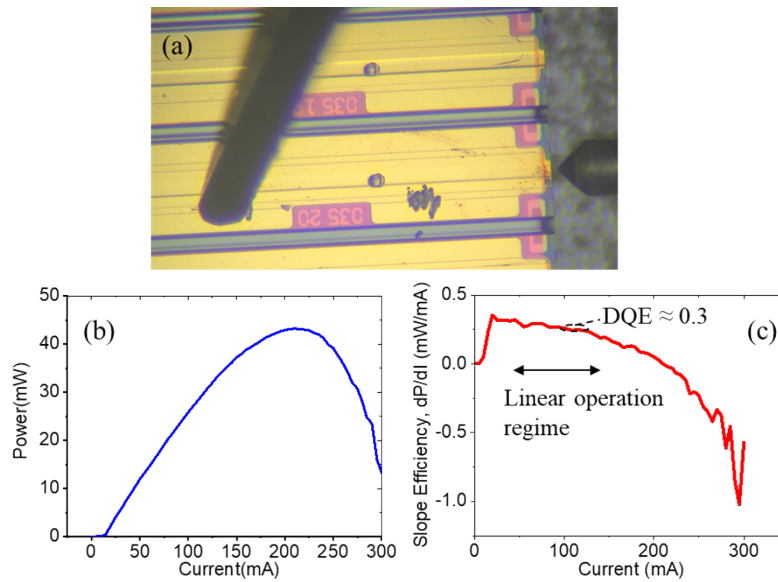


Fig. 3. (a) OM image of the DFB laser coupling. (b) L-I curve of the DFB laser and (c) the corresponding slope efficiency.

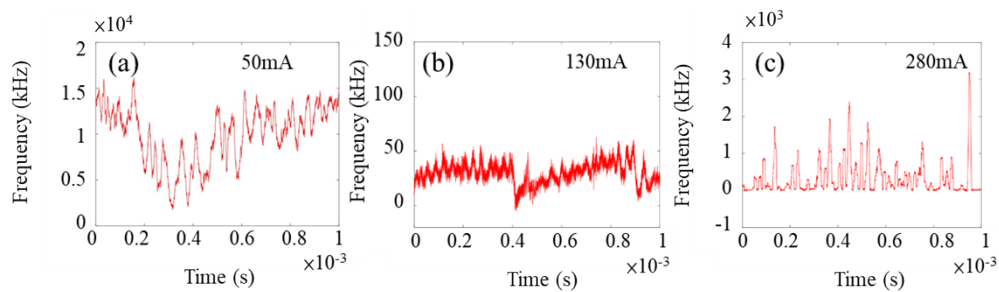


Fig. 4. Beating frequencies of self-heterodyne signals at (a) 50 mA, (b) 130 mA, and (c) 280 mA driving by a 1 kHz triangular waveform.

130 mA to 180 mA, while the corresponding sweeping frequencies (blue lines) are shown in Figs. 5(e)-5(h). An ideal, linear trace (red lines) is shown in these figures for comparison. We can observe that, for sweeping without linearization, the beating frequency is not a constant (Fig. 5(a)) and the frequency sweeping is not ideally linear for both up- and down-chirped periods (Fig. 5(e)), resulting in uncertainty in determining the position and velocity of 4-D FMCW LiDAR. With iteratively pre-distorted steps (Fig. 5(b)-(d)) and the pre-distorted waveforms (yellow lines), a better constant beating frequency can be obtained suggesting a nearly linear frequency sweeping in Fig. 5(f)-(h). The beating frequency for LiDAR imaging is located at the baseband around 30 kHz.

Next, we study the LiDAR system based on bare DFB laser chips, sweeping with the pre-distorted waveform. We simultaneously image the velocity and distance by scanning the galvo mirrors into 40×40 pixel maps. Figures 6(a)-(c) show the measured distances and motions at different velocities (10 mm/s in Fig. 6(b) and 0.01 mm/s in Fig. 6(c)). The results confirm the validity of the given distances and velocities; in the meantime, the difference between distances and velocities can be distinguished based on the baseband beat note signals. Also, we notice

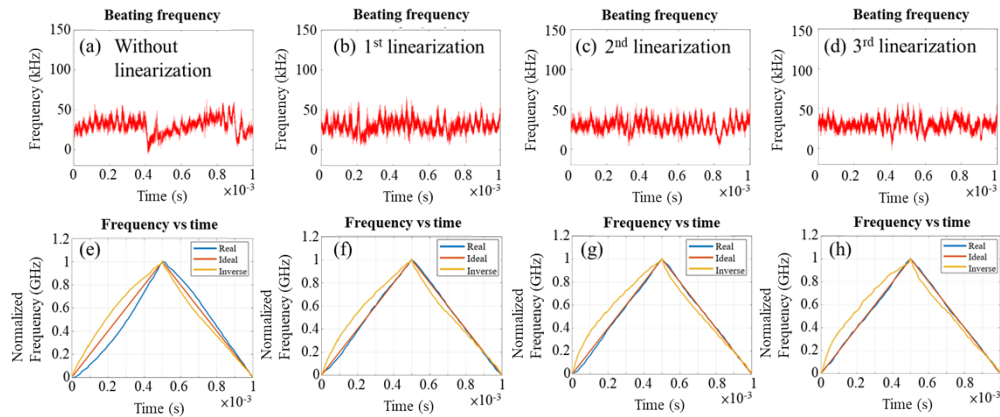


Fig. 5. (a-d) Beating frequencies of self-heterodyne signals with iterative linearization. (e-f) Corresponding reconstructed sweeping frequencies (blue lines), ideally linear curves (red lines), and the sweeping frequencies under pre-distorted waveforms (yellow lines).

the quality of velocity image gradually degrades with the decrease of velocity to ≈ 0.01 mm/s. This is because our low-frequency beat note signal with such a small Doppler shift frequency for slow-moving objects is easily screened by the background flicker noise of the DBF laser. A light source with superior low-frequency noise performance to that of a DFB laser is thus highly desired for the detection of slow-moving objects. We should also note that the hybrid FMCW mode is adapted for the 4D measurement detection of objects moving at an extremely low speed of 0.01 mm/s [8] while an extra duration of constant frequency after triangular frequency sweeps is generated for the analysis of a small Doppler frequency. Therefore, for the static targets ‘I’ and ‘U’, there would be no beating frequency available in the extra duration of the hybrid mode, and thus the targets cannot be observed in the velocity images.

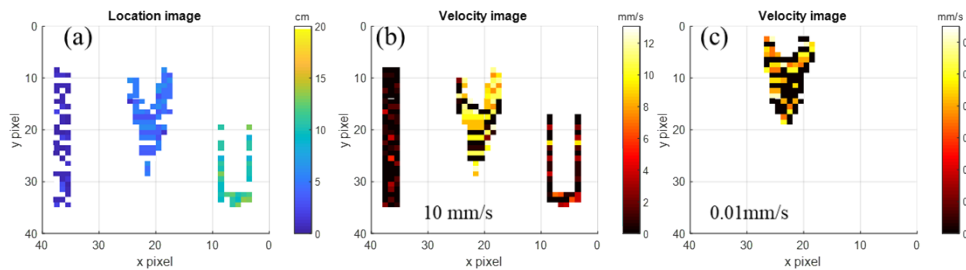


Fig. 6. (a) Images of measured distances. Images of velocities at (b) 10 mm/s and (c) 0.01 mm/s.

2.2. 4-D LiDAR imaging based on an external cavity laser (ECL)

Compared with the DFB laser, the ECL has been reported with a superior noise performance due to its external optical cavity can be realized with a much larger quality (Q) factor ($\sim 10^9$) than that of a semiconductor-based Bragg grating reflector [24,25]. We then replace the bare DFB laser with the commercial ECL to investigate the LiDAR performance at the baseband. The commercial ECL provides a narrower linewidth than that of our DFB one (≈ 50 vs. 250 kHz) while a sub-100 Hz linewidth has been previously reported on a realization of a heterogeneously

integrated, chip-scale semiconductor laser [24,25]. The same protocol of linearization of pre-distorted waveforms in Sec. 2.1 is again utilized for sweeping the driving current and modulating the laser frequency. Figures 7(a)-7(c) show the optimization results of the beating frequencies, and the corresponding sweeping frequencies (blue lines) are shown in Fig. 7(d)-7(f). An ideal, linear trace (red lines) is shown for comparison. Again, with the pre-distorted waveforms, a nearly linear frequency sweeping is achieved at the baseband around 120 kHz.

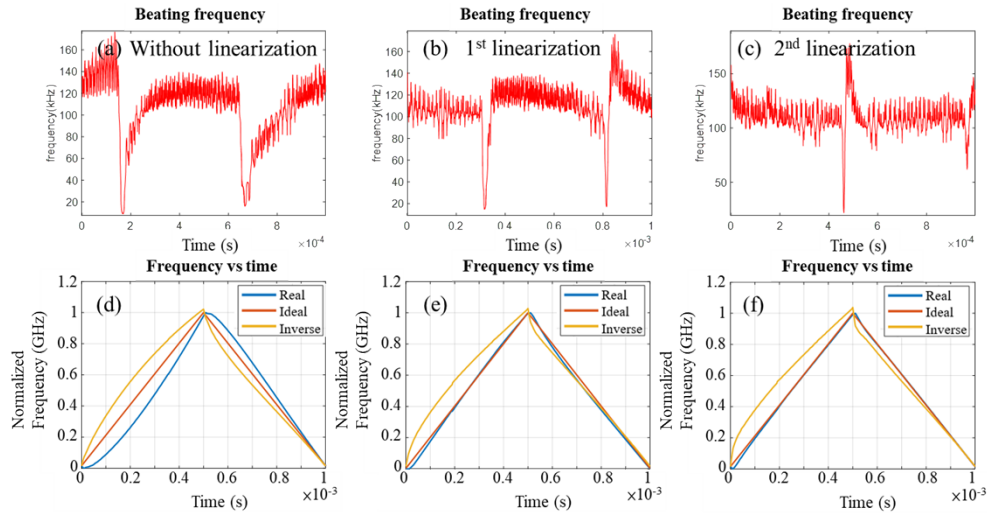


Fig. 7. (a-c) Beating frequencies of self-heterodyne signals with iterative linearization. (d-f) Corresponding reconstructed sweeping frequencies (blue lines), ideally linear curves (red lines), and the sweeping frequencies under pre-distorted waveforms (yellow lines).

Figures 8(a)-8(b) show the measured distance and motion at a velocity of 0.01 mm/s by sweeping with the pre-distorted waveform. In comparison with the DFB laser, we can see that the ECL shows a similar distinguishability in distances but a much better sensitivity at a low speed. For a more detailed comparison of the differences between the commercial ECL and the DFB laser, the baseband spectra of some pixels selected from \heartsuit -shaped symbols of Fig. 6 and Fig. 8 are plotted in Fig. 9.

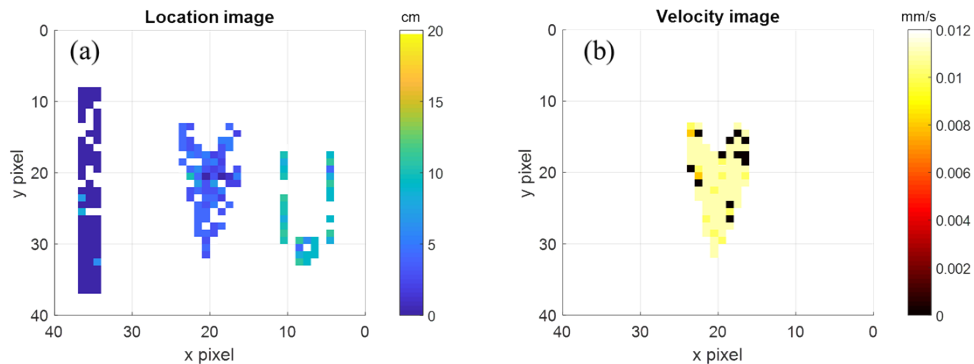


Fig. 8. Images of the measured (a) distance and (b) velocity at 0.01 mm/s.

The better signal-to-noise ratio of the ECL spectrum yields superior image quality and therefore higher velocity sensitivity of 4-D FMCW LiDAR. This result can be attributed to that the high-Q

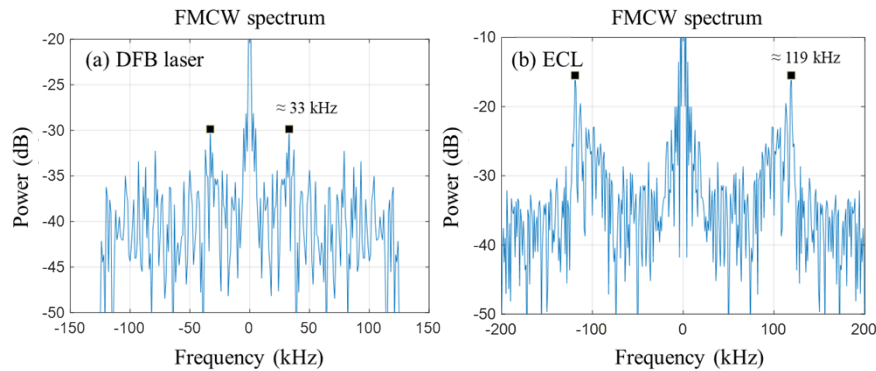


Fig. 9. Baseband spectra measured at the pixels selected from \heartsuit -shaped symbols of the (a) DFB laser and (b) ECL.

external cavity suppresses the low-frequency noise for FMCW LiDAR applications [23]. It is also worth noting that the current modulation of DFB lasers and ECLs can generate different sweeping slopes, thus yielding distinct beat frequencies, even when utilizing the same delay length. The primary objective is to adjust the beat frequency at the baseband to around 100 kHz, aiming to minimize the effects of flicker noise.

2.3. Real-time LiDAR based on MEMS mirrors with high velocity sensitivity

To examine and compare the abilities of the 4-D LiDAR at the baseband, we now demonstrate a real-time LiDAR system for mapping the images again with the ECL due to its superior performance in low-frequency noise to that of DFB as previous discussion. In our scanning system relying on galvo mirrors, we stop the mirror movement at each pixel during the acquisition of the FMCW spectra. Approximately, several hours are required to capture a 40×40 pixel map with our galvo-mirror-based 4-D LiDAR system. Despite achieving high velocity sensitivity from the above demonstrations, this is unsuitable for a real-time LiDAR system, thereby constraining the system's imaging capabilities and applications. Here, to improve the sampling rate of 4-D LiDAR images, a miniature, linear mode, and electromagnetically driven two-dimensional scanning MEMS mirror (Hamamatsu, S13124-01) is used to offer both compact and fast image scanning. The field of view (FOV) of the MEMS mirror is 20° . We align the fast axis of the MEMS mirror along the x direction and the slow axis along the y direction. Images are taken line by line in the x direction in a zigzag manner. A multifunctional data acquisition system (DEWETRON Inc., DEWE3-RM4) with 2 Ms/s sampling rate is also equipped to enable fast data acquisition. The same ECL with linearization processes is again adapted for real-time 4-D LiDAR demonstration. We first image the location and velocity with a frame rate at 1 fps. Thanks to the MEMS and data acquisition system, higher pixel resolution can be imaged within a short period of time. Figures 10 show the images of distances and velocities in 50×40 pixel mapping. For the LiDAR images by MEMS, the relative distance between the I and U targets was set at 15 cm while the \heartsuit -shaped object was moving in-between during the measurement process. We can see that, with the fast image acquisition, the position can be distinguished, and the velocity is marginally resolved even at a relatively higher speed 40 mm/s.

There are two challenges in realizing high velocity sensitivity for a fast frame rate. The first challenge is the limited scanning time. The frequency ramping period (in sub-ms) during laser sweeping must be shortened to fit the short trigger time per pixel, which sacrifices the velocity resolution. Also, the 2 Ms/s sampling rate of our current data acquisition system limits the available ramping period for each pixel. Therefore, there would be a trade-off between pixel

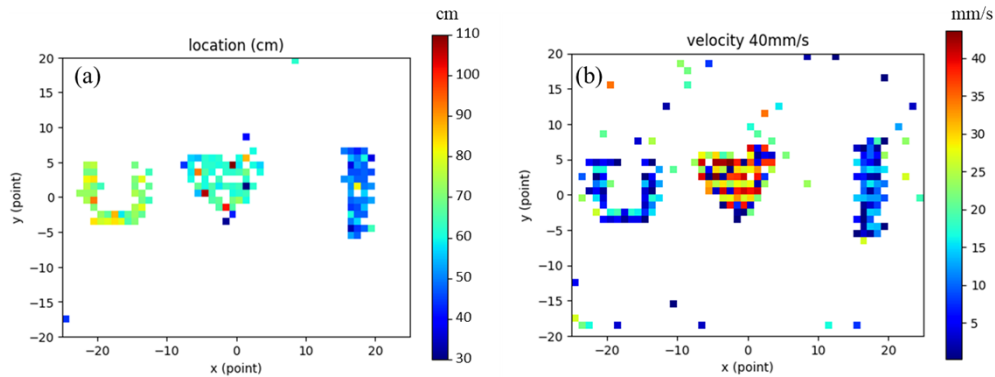


Fig. 10. Images of the measured (a) distance and (b) velocity at 40 mm/s for a 1 fps. The mapping is in 50×40 pixels.

numbers (image resolution), velocity sensitivity, and frame rates. The second challenge is that instead of keeping the mirrors static when recording the beat notes in our galvo-mirror-based systems, the setup with the MEMS mirror records the beat notes continuously while the mirror is moving. Because the beam movement can also induce the Doppler effect, the mechanical ringing of the MEMS mirror can also cause in fluctuations in the detected velocity.

To alleviate these issues, we adjust the aspect ratio of the scanning images and reallocate more time along the x-axis to slow down the mirror movement along the fast axis while keeping the same frame rate. A slower mirror scanning speed helps to improve the velocity sensitivity and resolution of our targeted images. Figures 11 show the images of distances and velocities in a 100×20 pixel mapping with 1 fps. The scanning velocity along the x-axis is half the speed compared to that of a 50×40 pixel mapping. Now, both the location and velocity can be accurately identified with a doubled resolution along the x-axis.

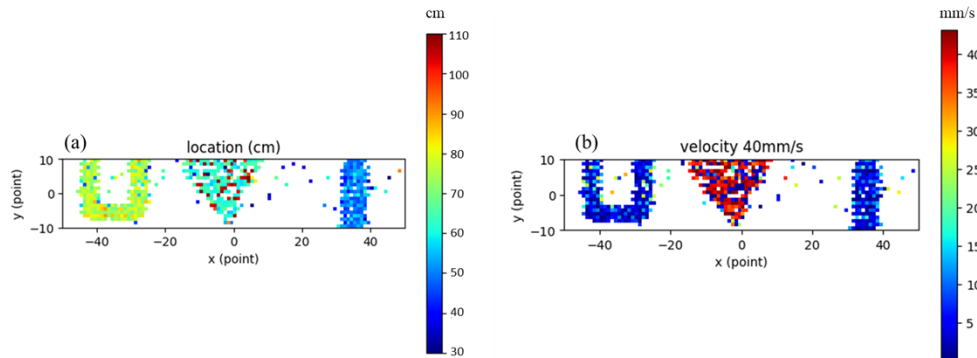


Fig. 11. Images of the measured (a) distance and (b) velocity at 40 mm/s for a frame rate at 1 fps. The mapping is in 100×20 pixels.

Figures 12 show the velocity histograms of the moving pixels at 40 mm/s for both 100×20 pixel and 50×40 pixel mappings, related to that in Fig. 11(b) and 10(b), respectively. Clearly, the 100×20 pixel mapping exhibits a smaller error and higher precision in determining the velocity. The root-mean-square error (RMSE) reduces from 13.28 mm/s to 9.24 mm/s.

Last, we investigate the limit on the velocity sensitivity by real-time mapping the velocities at 10 mm/s, 5 mm/s, and 2 mm/s. Figures 13 show the corresponding images of distances and velocities in a 100×20 pixel mapping for 1 fps. High velocity sensitivity can be realized even

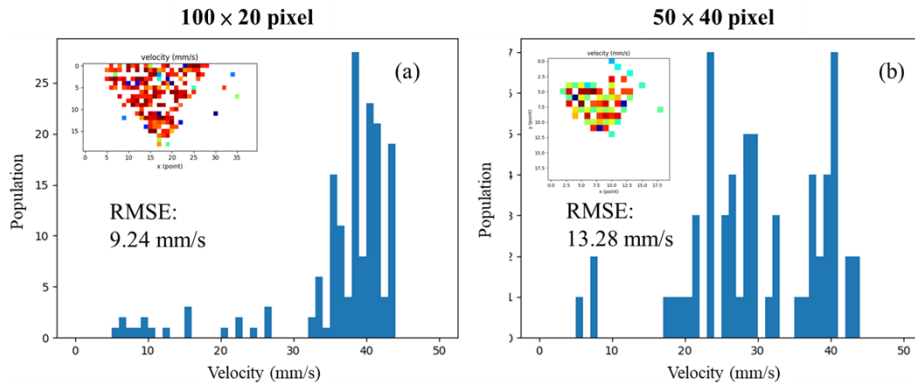


Fig. 12. Velocity histograms of the moving pixels at 40 mm/s for both (a) 100×20 pixel and (b) 50×40 pixel mappings.

down to 5 mm/s, while at 2 mm/s, the velocity is barely distinguished. Due to the constrained sampling rate of the multifunctional data acquisition system, the hybrid mode is prohibited in the real-time LiDAR measurement.

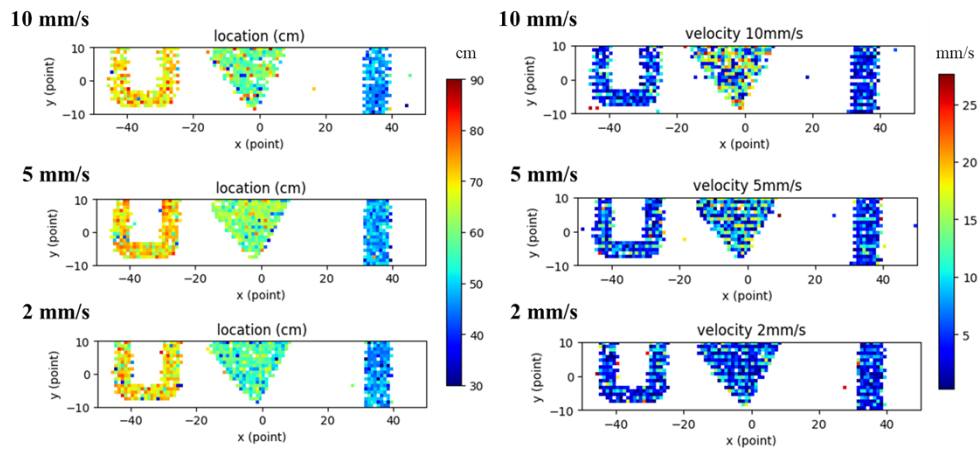


Fig. 13. Images of the measured distances and velocities at 40 mm/s for a frame rate at 1 fps. The mapping is in 100×20 pixels.

This demonstration provides the potentials to develop a 4-D LiDAR system in a fast, compact, and real-time scheme with high velocity sensitivity down to 10 mm/s. Moreover, we note that the trade-off between resolution, frame rate, and sensitivity can be later improved by utilizing an ultra-narrow linewidth ECL [24,25] and a data acquisition system with a higher sampling rate.

3. Conclusion

To conclude, we demonstrate 4-D FMCW LiDAR based on both a conventional bare DFB laser and a commercial ECL. By the beat notes at the baseband (as low as 100 kHz), high velocity sensitivity at 0.01 mm/s can be obtained without the need of MOD for up-converting frequencies and costly high-speed processing. Real-time LiDAR imaging at 1 fps is achieved through the utilization of a MEMS scanner. Both location and velocity (down to 10 mm/s) are resolved by optimizing the MEMS imaging window. This study unveils the potential of a compact, rapid, and cost-effective 4-D FMCW LiDAR system for diverse applications.

Funding. National Science and Technology Council (101-2221-E-009-011-MY3, 111-2221-E-A49-014-MY3, 112-2221-E-008-064, 112-2622-8-008-004); Ministry of Economic Affairs (98-EC-17-A-07-S1-001).

Acknowledgments. P.-H. W. acknowledges the research financial support from the National Science and Technology Council (NSTC), Taiwan under grant number 112-2221-E-008-064 and 112-2622-8-008-004.

Disclosures. The authors declare no conflicts of interest.

Data availability. Data underlying the results presented in this paper are not publicly available at this time but may be obtained from the authors upon reasonable request.

References

1. L. Thobois, J. P. Cariou, and I. Gultepe, "Review of lidar-based applications for aviation weather," *Pure Appl. Geophys.* **176**(5), 1959–1976 (2019).
2. D. M. Winker, R. H. Couch, and M. P. McCormick, "An overview of LITE: NASA's Lidar In-space Technology Experiment," *Proc. IEEE* **84**(2), 164–180 (1996).
3. H. Nehme, C. Aubry, T. Solatges, *et al.*, "LiDAR-based structure tracking for agricultural robots: application to autonomous navigation in vineyards," *J. Intell. Robot Syst.* **103**(4), 61 (2021).
4. S. Gargoum and K. El-Basyouny, "Automated extraction of road features using LiDAR data: A review of LiDAR applications in transportation," *Proc. 4th Int. Conf. Transp. Inf. Saf. (ICTIS)*, 563–574 (2017).
5. E. Arnold, O. Y. Al-Jarrah, M. Dianati, *et al.*, "A survey on 3D object detection methods for autonomous driving applications," *IEEE Trans. Intell. Transp. Syst.* **20**(10), 3782–3795 (2019).
6. R. Whyte, L. Streeter, M. J. Cree, *et al.*, "Application of lidar techniques to time-of-flight range imaging," *Appl. Opt.* **54**(33), 9654–9664 (2015).
7. B. Behroozpour, P. A. M. Sandborn, M. C. Wu, *et al.*, "LiDAR system architectures and circuits," *IEEE Commun. Mag.* **55**(10), 135–142 (2017).
8. Y.-X. Lin, Z. Ahmad, S.-Y. Ou, *et al.*, "A 4-D FMCW LiDAR with ultra-high velocity sensitivity," *J. Lightwave Technol.* **41**(21), 6664–6674 (2023).
9. S. Suyama, H. Ito, R. Kurahashi, *et al.*, "Doppler velocimeter and vibrometer FMCW LiDAR with Si photonic crystal beam scanner," *Opt. Express* **29**(19), 30727–30734 (2021).
10. Y. Xue, Y. Niu, and S. Gong, "External modulation optical coherent domain reflectometry with long measurement range," *Sensors* **21**(16), 5510–5517 (2021).
11. W. Yi, Z. Li, Z. Zhou, *et al.*, "Frequency-modulated chirp signals for single-photodiode based coherent LiDAR system," *J. Lightwave Technol.* **39**(14), 4661–4670 (2021).
12. N. Yokota, H. Kiuchi, and H. Yasaka, "Directly modulated optical negative feedback lasers for long-range FMCW LiDAR," *Opt. Express* **30**(7), 11693–11703 (2022).
13. Y. Wu, L. Deng, K. Yang, *et al.*, "Narrow linewidth external cavity laser capable of high repetition frequency tuning for FMCW LiDAR," *IEEE Photonics Technol. Lett.* **34**(21), 1123–1126 (2022).
14. Y. Yoshikuni and G. Motosugi, "Multielectrode distributed feedback laser for pure frequency modulation and chirping suppressed amplitude modulation," *J. Lightwave Technol.* **5**(4), 516–522 (1987).
15. Z. Li, P. Dai, L. Meng, *et al.*, "An ultrafast wavelength-swept REC-DFB laser based on the instantaneous injection current," *2022 Asia Communications and Photonics Conference (ACP)*, 1576–1578 (2022).
16. J. Yang, Y. Meng, X. Hu, *et al.*, "High-ranging-precision FMCW LiDAR with adaptive pre-distortion of current injection to a semiconductor laser," *J. Lightwave Technol.* **42**(6), 1870–1876 (2024).
17. X. Zhang, J. Pouls, and M. C. Wu, "Laser frequency sweep linearization by iterative learning pre-distortion for FMCW LiDAR," *Opt. Express* **27**(7), 9965–9974 (2019).
18. A. van der Ziel, "Noise in solid-state devices and lasers," *Proc. IEEE* **58**(8), 1178–1206 (1970).
19. Mikiya Kamata, Yosuke Hinakura, and Toshihiko Baba, "Carrier-suppressed single sideband signal for FMCW LiDAR using a Si photonic-crystal optical modulators," *J. Lightwave Technol.* **38**(8), 2315–2321 (2020).
20. S. Hu, P. Srinivasan, and M. Rezk, "Coherent LiDAR Technology: practical deployment and challenges," in *Optical Fiber Communication Conference (OFC) 2023, Technical Digest Series* (Optica Publishing Group, 2023), paper M3F.5.
21. G. Zhang, Z. Ding, K. Wang, *et al.*, "Demonstration of high output power DBR laser integrated with SOA for the FMCW LiDAR system," *Opt. Express* **30**(2), 2599–2609 (2022).
22. Z. Ahmad, S.-I. Kuo, Y.-C. Chang, *et al.*, "Avalanche photodiodes with dual multiplication layers and ultra-high responsivity-bandwidth products for FMCW Lidar system applications," *IEEE J. Sel. Top. Quantum Electron.* **28**(2: Optical Detectors), 1–9 (2022).
23. T. J. Ahn, J. Y. Lee, and D. Y. Kim, "Suppression of nonlinear frequency sweep in an optical frequency-domain reflectometer by use of Hilbert transformation," *Appl. Opt.* **44**(35), 7630–7634 (2005).
24. W. Liang, V. S. Ilchenko, D. Eliyahu, *et al.*, "Ultralow noise miniature external cavity semiconductor laser," *Nat. Commun.* **6**(1), 7371 (2015).
25. W. Jin, Q.-F. Yang, L. Chang, *et al.*, "Hertz-linewidth semiconductor lasers using CMOS-ready ultra-high-Q microresonators," *Nat. Photonics* **15**(5), 346–353 (2021).